Over 800% efficiency enhancement of all-inorganic quantum-dot light emitting diodes with an ultrathin alumina passivating layer r

Wenyu Ji,[1*] **Huaibin Shen**, [2*] **Han Zhang**,[a] **Zhihui Kang**,[1] **Hanzhuang Zhang** [1*]

[1]*Key Lab of Physics and Technology for Advanced Batteries* (*Ministry of Education*), *College of Physics, Jilin University, 2699 Qianjin Street, Changchun, 130033, China*
[2]*Key Laboratory for Special Functional Materials of Ministry of Education, Henan University, Kaifeng 475004, China*

Abstract

The use of robust, inorganic charge-transport materials is always desired in quantum-dot light emitting diodes (QLEDs) because they are expected to allow higher stability and less cost than that of organic counterparts. We achieve here an all-inorganic QLED with excellent efficiency by modifying a solution-processed NiO (s-NiO) surface with an ultrathin Al_2O_3 passivating layer. The localized electric field induced by nickel oxyhydroxide (NiOOH) is estimated to be ~70 MV/cm at a distance of 6 nm from the s-NiO layer. Both transient resolution photoluminescence and X-ray photoelectron spectroscopy measurements demonstrate that the Al_2O_3 layer can effectively passivate the NiOOH on the s-NiO surface, thereby suppressing exciton quenching. This improves the highest efficiency of the QLED without Al_2O_3 layer by over 800% to an external quantum efficiency of 34.1 cd/A (8.1%), making it the best-performing all-inorganic QLED.

Keywords: QLED; all-inorganic; passivating layer; localized electric field; exciton quenching

1. Introduction

Semiconductor quantum-dots (QDs) exhibit unique physical and chemical properties,[1-4] including a tunable bandgap and narrow emission at UV to near-infrared frequencies, high quantum yield, low-cost solution-based manufacture, and good photo-stability. They are therefore promising materials for the next generation of solution-processed optoelectronics.[5-7] They have been studied for potential use in lighting and display technologies; e.g., QDs could be used as color converting materials or as the emissive layer in sandwiched electroluminescence (EL) devices.[8-15] Especially, the electrically driven QD light emitting diodes (QLEDs) have been emerging as an important technology to improve the performance of lighting and display systems due to their wider color gamut and cheaper solution-based manufacture compared with organic LEDs.[16-21] The most efficient QLEDs have been achieved with a hybrid architecture employing QD layers sandwiched between an organic hole-transport layer (HTL) and an inorganic metal oxide (e.g., ZnO nanoparticles[5,17,18,22-24] and sol-gel TiO_2[25-27]) electron-transport layer (ETL). While Cd-based hybrid QLEDs perform comparably to state-of-the-art organic light emitting diodes at the lab scale,[5,17-20] they still depend on organic small molecule or polymer HTLs that are more sensitive to oxygen and moisture than purely inorganic materials.

Fabrication of an efficient QLED with all-inorganic charge transport layers (CTLs) and no organic material is desired and necessary for various lighting and display applications. In general, inorganic metal oxides are resistant to various organic solvents, and so should form a QD layer with a high-quality CTL/QDs interface. NiO is a popular

and effective hole transport material for all-inorganic QLEDs due to its outstanding optical transparency and stability.[28-30] The first inorganic QLED with a radiofrequency-sputtered NiO HTL was reported by Bawendi *et al.* in 2008; it showed a maximum current efficiency (external quantum efficiency, EQE) of 0.064 cd/A (0.1%) and peak luminance of 1950 cd/m^2.[28] To overcome problems of high cost and incompatibility with solution processing of radiofrequency sputtering, Mashford *et al.* developed the first solution-processed inorganic QLED in 2009.[31] However, its performance was rather low, with a maximum EL brightness (current efficiency) of 249 cd/m^2 (0.014 cd/A). All-inorganic QLEDs still underperform hybrid ones, and the underlying physical reasons limiting their performance need to be fully understood before they can be improved. The poor performance of NiO-based all-inorganic QLEDs has been attributed to exciton quenching induced by the many free carriers and defects/traps on the surface of adjacent inorganic NiO HTLs.[28-30]

To alleviate quenching interactions, two types of strategies have been proposed: growing thick shells outside the QD cores or inserting an exciton blocking or insulating layer to separate spatially the QD layer from the metal oxide layer.[5,30, 32,33] The excitons in QDs can be quenched by plasmon modes or QD charging when QDs are directly deposited on NiO film.[28,29,31,34] A better understanding of the mechanisms responsible for QD emission quenching would more fully characterize NiO HTLs, and thus help improve all-inorganic QLEDs. Two main approaches can be employed to reduce the quenching of excitons in QDs/inorganic HTLs. The first is to construct a high-quality inorganic HTL with low defect/trap density, but this remains challenging.

The other is to introduce a buffer layer to passivate the defects/traps on the inorganic HTL, spatially separating it from the QDs. This is a simple and feasible way to suppress exciton quenching at the QDs/inorganic HTL interface. We recently reported a highly efficient all-inorganic green QLED with a solution-processed Al_2O_3 spacing layer. Its maximum efficiency was 20.5 cd/A,[30] which is much lower than that of the best hybrid QLEDs.[5,17,18,22-24] The origin of the emission quenching induced by NiO is debated. Therefore, both device optimization and quenching mechanisms need to be investigated to achieve efficient all-inorganic QLEDs.

This work reports the first all-inorganic QLED to reach an efficiency of 34.1 cd/A. It employs solution-processed NiO (s-NiO) and ZnO nanoparticles as CTLs. The interactions between the QDs and s-NiO are also explored. A significant contribution to the efficiency improvement originates from the successful introduction of an ultrathin insulating Al_2O_3 passivating layer obtained by atomic layer deposition (ALD). This layer effectively passivates the nickel oxyhydroxide (NiOOH) species on the s-NiO surface, which dramatically suppresses QD charging in the QLEDs and greatly enhances the device performance. The current efficiency of the device with a 2 nm Al_2O_3 passivating layer is ~8.7 times that of the control device.

2. Results and Discussion

In inorganic QLEDs without an Al_2O_3 layer, the electrons and holes accumulate at the s-NiO/QDs interface according to the energy level alignment of the device, as shown in **Figure S1** in the **Supporting Information**. There they will form excitons, and then

release their energy by photon emission or other nonradiative processes. Therefore, the s-NiO/QDs interface is vital to both QD emission dynamics and device performance. Armstrong *et al.*[35] found that many dipolar NiOOH surface species were present on the surface of pristine s-NiO films, leading to the presence of unique surface dipoles from the predominantly hydroxylated O–Ni–OH surface. The dipoles induce a strong localized electric field at the surface of the s-NiO layer. The electric field strength near a NiOOH dipole moment can be estimated as follows:[36]

$$E = \frac{1}{4\pi\varepsilon_0 r^3}(3(\vec{\mu}\cdot\hat{r})\hat{r} - \vec{\mu}) \approx -\frac{\vec{\mu}}{4\pi\varepsilon_0 r^3} \quad (1)$$

where E is the electric field intensity, ε_0 is the permittivity of free space, r is the distance to the dipole, and μ is the dipole moment. Considering the average diameter (~12 nm) of the QDs used here, it is rational to assess the effect of the electric field on exciton emission dynamics by estimating the field intensity at a distance of 6 nm from the s-NiO surface. Taking the calculated density functional theory value of 2.9 debye for the NiOOH molecule gives an electric field strength of ~70 MV/cm at 6 nm from the s-NiO layer. Provided that the electric field is uniformly distributed in the device, the intensity of the localized electric field is equivalent to applying a 7 V bias to a QLED with a total thickness of 100 nm between two electrodes. Such a strong electric field should facilitate radiationless decay channels with charge-transfer/charging processes, leading to severely decreased device efficiency. Therefore, passivating the NiOOH on the surface of the s-NiO layer should feasibly improve device performance.

An insulating Al_2O_3 layer is employed here to passivate the NiOOH on the s-NiO surface. The device structure is schematically shown in **Figure 1**a, and the passivating

mechanism is given in Figure 1b. The Al_2O_3 passivating layer is obtained by ALD, a method similar to chemical vapor deposition (**Figure S**2). The thickness of the Al_2O_3 film deposited on s-NiO can be controlled at the atomic level by alternating exposure cycles of $Al(CH_3)_3$ and H_2O.[37,38] Moreover, Al_2O_3 films with good uniformity over large substrates and excellent conformality on three-dimensional surface topologies can be obtained by ALD. To assess the effect of the Al_2O_3 passivating layer on the s-NiO surface, X-ray photoelectron spectroscopy (XPS) is performed; $Ni_{3/2}$ spectra for s-NiO and s-NiO/Al_2O_3 (2 nm) films are shown in **Figure** 2. The content of Ni^{2+} (i.e., NiO) clearly increases upon deposition of the Al_2O_3 passivating layer. This may be due to the consumption of hydroxyl (–OH) in the NiOOH species during exposure to $Al(CH_3)_3$ deposition cycles. The integral area from the XPS spectra for the NiOOH fractions in films with and without an Al_2O_3 layer are 1.39 and 1.59, respectively, which indicates a clear decrease in NiOOH species after Al_2O_3 deposition. These results further demonstrate that the deposition of an Al_2O_3 layer can effectively passivate NiOOH species on the s-NiO surface, and thus suggest that s-NiO/Al_2O_3 will be suitable as the HTL for all-inorganic QLEDs.

Given the strong insulating properties of Al_2O_3, the thickness of the passivating layer will significantly influence the device performance.[5] ALD allows precise thickness control (the Al_2O_3 layer grows by ~0.09 nm each deposition cycle), thus ensuring the reproducibility and yield of the devices, which are two important properties for the commercialization of QLEDs. The morphologies of the s-NiO films with and without an Al_2O_3 layer are assessed by atomic force microscopy (AFM,

Figure 3). Al_2O_3 deposition resulted in a slight smoothing of the s-NiO film: root-mean-square (RMS) roughness values are 1.62, 1.58, and 1.43 nm for pure s-NiO, s-NiO/Al_2O_3 (0.45 nm), and s-NiO/Al_2O_3 (0.9 nm), respectively. An AFM image of pure ITO substrate (RMS roughness 1.92 nm) is shown in **Figure S3**. Thus, s-NiO deposition smoothed the ITO substrate. Of note, the smoothing effect of Al_2O_3 reaches a limit, past which roughness does not decrease upon further Al_2O_3 deposition. For example, Figure 3d shows s-NiO/Al_2O_3 (1.45 nm) to have an RSM roughness of 1.43 nm, which is identical to that of s-NiO/Al_2O_3 (0.9 nm). This is attributed to the excellent conformality of the ALD Al_2O_3 layer on three-dimensional surface topologies. The first few Al_2O_3 monolayers (<0.9 nm) (in addition to passivating the NiOOH) smooth the s-NiO surface so effectively that any further Al_2O_3 layers do not affect the morphology of the surface.

Scanning electron microscopy (SEM) shows high-quality QD layers on both s-NiO and s-NiO/Al_2O_3 (0.9 nm) substrates (**Figure S4**), demonstrating that the Al_2O_3 layer has no effect on the formation of the QD film. The passivating effect of Al_2O_3 is demonstrated by fluorescent microscopy (Figure S4c and S4d) images of QD layers on s-NiO and s-NiO/Al_2O_3 (0.9 nm) substrates. (Note that both images are obtained under the same conditions: i.e., both samples are simultaneously fixed on the sample holder of the fluorescent microscope, and then the images are taken with the same excitation source.) The QDs on s-NiO/Al_2O_3 (0.9 nm) clearly exhibit higher emission intensity than those on pristine s-NiO, indicating that the Al_2O_3 layer suppresses the quenching of QD emission by passivating the s-NiO layer. Fluorescent microscopy of the QD layer

on UV‑ozone-treated s-NiO film reveals much weaker photoluminescence (PL) intensity than that from pristine s-NiO or s-NiO/Al_2O_3 (0.9 nm) films (data not shown). UV‑ozone treatment has been reported to increase the amount of NiOOH species on the s-NiO surface.[43] These results further demonstrate that the quenching of QD emission is derived from strong dipolar NiOOH species.

Figure 4 shows the photoelectrical properties of the all-inorganic QLEDs. Their current densities decrease with increasing Al_2O_3 thickness for a given operating voltage. Vibrating-head Kelvin probe measurements were implemented for the pristine NiO film and NiO with different Al_2O_3 insulating layers. The estimated work function is -5.25 eV for pristine NiO and -5.20 to -5.30 eV for NiO with different Al_2O_3 layers. That is, the work function of HTLs is independent on the Al_2O_3 insulating layers. These results indicate that the decreased current density for devices with increasing Al_2O_3 insulating layer thicknesses is not due to the barrier to hole injection from HTL to QDs but due to the excellent insulating properties of the ALD Al_2O_3 layer. Notably, the current densities show a marked decrease in the region of low driving voltages (<3 V; Figure 4a), which is attributable to the reduction in leakage current (electrons) from QDs to the s-NiO HTL. Device C, with a 0.9 nm Al_2O_3 layer, achieved the greatest luminance (14,713 cd/m^2; Figure 4b), which is three times that of device A (4716 cd/m^2), with pristine s-NiO as the HTL. Device C also showed the greatest current efficiency (34.1 cd/A), which is 865% higher than that of device A (3.8 cd/A). The corresponding EQE enhancement is 861% (from 0.94% to 8.1%). The current-voltage characteristics of electron- and hole-only devices show that the hole injection into the device is similar

to the electron injection for the device without Al_2O_3 passivating layer as shown in **Figure S5** (**Supporting Information**). The introduction of Al_2O_3 passivating layers decreases the hole injection from HTL to QDs, which makes a imbalanced carrier (holes and electrons) injection into the devices, hence aggravating the efficiency roll-off behavior as shown in figure 4c. However, the device containing the Al_2O_3 passivating layers present higher efficiency than that without this passivating layer, which indicates that, comparing with the hole injection, the emission quenching induced by NiO plays a more significant role in deciding the performance of NiO based all-inorganic QLEDs. All the results show that the Al_2O_3 passivating layer plays two critical roles in enhancing performance: (i) it suppresses the quenching of QD emission by passivating the NiOOH on the surface of the s-NiO film; (ii) it reduces the leakage current of electrons from QDs to the s-NiO HTL.

Spectroscopic measurements for the QDs are shown in **Figure 5**, and the peak wavelength of the EL/PL spectra and PL decay lifetimes of the QDs are given in detail in **Table 1**. Figure 5a shows that each QLED exhibits pure green emission without any other parasitic contribution, indicating that most of the excitons are formed in the QDs, regardless of Al_2O_3 insertion. The emission spectrum of QDs on a glass substrate is red-shifted (from 522.4 to 526.2 nm) relative to that in toluene, which is consistent with previously reported findings for interactions between different particles.[24,30,44-45] However, Figure 5a shows a significant and interesting phenomenon in that the EL spectrum for device A is red-shifted (peaking at 530.0 nm) compared with the emission spectrum of QDs on a glass substrate. However, the EL spectra become blue-shifted as

the thickness of the Al_2O_3 layer increases. Finally, when a 0.9 nm Al_2O_3 passivating layer is deposited on an s-NiO HTL, the EL spectrum is similar to that of QD film on a glass substrate. Similarly, the blue-shift trend also emerges for the PL spectra of QD films on s-NiO and s-NiO/Al_2O_3 layers (Figure 5c). The differences in the EL/PL spectra clearly originate from interactions between the QDs and the s-NiO. The red shift observed here has been observed previously when QDs are subjected to a strong electric field due to the Stark effect;[39-42] however, this may be not the case here. As Figure 5b shows, the EL spectra for device C under different applied voltages exhibit identical profiles, thus revealing that any effect of the extrinsic electric field on the red shift of the EL spectra can be ignored in the present case. Therefore, the observed red-shifting must be induced by other mechanisms. The charging of QDs can red shift their emission spectrum.[44-45] In our devices, the localized electric field of NiOOH dipoles must lead to a permanent charging state for the QDs close to the s-NiO surface. Compared with the PL spectrum of QDs on glass, the large red shift of the EL spectrum of device A can be attributed to the substantial charging of QDs owing to the strong localized electrical field induced by NiOOH. The introduction of an Al_2O_3 layer passivates the NiOOH species and suppresses the red-shifting of the EL/PL spectra; hence, a trend of blue-shifting emerges (Figure 5a and 5c).

To verify the above, we carried out time-resolved PL (TRPL) measurements (Figure 5d and **Figure S6** the in Supporting Information). Compared with QDs in solution, the PL decay lifetime of excitons for QD film on glass is slightly shortened (from 15.01 to 13.42 ns), which is likely due to previously reported interactions

between QDs.[24,30,46-47] In comparison, the exciton lifetime is dramatically decreased to 9.85 ns when the QDs are deposited on the s-NiO directly, because the s-NiO layer induces another nonradiative path and/or a strong localized electric field. When an Al_2O_3 passivating layer is inserted between the s-NiO and the QDs, the PL decay lifetimes greatly increase owing to the suppression of nonradiative processes. The steady-state PL spectra also indicate that the emission from QDs is effectively recovered with an ultrathin Al_2O_3 passivating layer on the s-NiO. These results further demonstrate that the interactions between QDs and s-NiO can be reduced by passivating NiOOH on the NiO surface.

3. Conclusion

A powerful method to passivate an s-NiO surface was demonstrated. It allowed the efficient, simple, and facile fabrication of all-inorganic QLEDs, which showed a current efficiency (EQE) of 34.1 cd/A (8.1%). This was obtained by depositing an insulating Al_2O_3 passivating layer on an s-NiO film, representing an efficiency enhancement of over 800% relative to a device employing a pristine s-NiO HTL. Furthermore, the device performance is comparable to that of QLEDs with a hybrid structure. Exploration of the interactions between s-NiO and QDs showed that quenching of QD emission on s-NiO correlated with the permanent charging of the QDs due to the intense electric field induced by NiOOH. XPS results demonstrated that an ultrathin Al_2O_3 layer can effectively passivate the NiOOH by reducing it to NiO, which reduced the effect of the localized electric field induced by NiOOH on the QD emission.

Transient and steady-state PL measurements also indicated that the Al_2O_3 layer effectively protected the excitons in the QDs from quenching by the s-NiO. This work demonstrates for the first time the origin of QD emission quenching on s-NiO, and suggests a way to achieve all-inorganic QLEDs potentially suitable for lighting and full-color panel displays.

4. Experimental Section

4.1 Preparation of green QDs and all-inorganic QLEDs. QDs with a ZnCdSSe/ZnS core/shell structure were synthesized according to an established method.[48] The optical and morphological properties of the QDs have been reported previously.[30] The QDs are on average ~12 nm in diameter and exhibit a green emission with a peak at 527 nm. The QLEDs (**Figure 1a**) consist of glass-coated ITO/s-NiO (~50 nm)/Al_2O_3 (*x* nm)/QDs (~25 nm)/ZnO (~40 nm)/Al (100 nm). The s-NiO, QDs, and ZnO are used as the HTL, emission layer, and ETL, respectively. The Al_2O_3 layer is deposited by alternating exposures of $Al(CH_3)_3$ and H_2O on the same substrate maintained at 150 °C; its thickness increases by ~0.09 nm with each ALD cycle. Different thicknesses of Al_2O_3 layers are deposited on s-NiO films to make devices A (0 nm), B (0.45 nm), C (0.9 nm), and D (1.35 nm). Note that device A is a control device without an Al_2O_3 interlayer. Before fabricating the devices, the ITO substrates were ultrasonically cleaned by a standard procedure of acetone, ethanol, deionized water, and isopropanol followed by *ex situ* UV ozone treatment in air for 5 min.

The s-NiO film was obtained according to the method reported by So *et al*.[49] To prepare the precursor solution, we dissolved nickel acetate tetrahydrate ($Ni(OAc)_2 \cdot 4H_2O$, Aldrich) and an equimolar quantity of monoethanolamine (Aldrich) in ethanol. This precursor solution (30 mg/ml) was spin-coated onto the UV–ozone-treated ITO substrates at 2000 rpm, and then annealed at 275 °C for 45 min in air to obtain a highly conductive layer of ~50 nm thickness. The QD layers were obtained by spin-coating QDs in toluene (18 mg/ml) at 2000 rpm and annealing at 70 °C for 30 min in a glove box (MBRAUN). The ZnO ETLs were also deposited by spin-coating a 30 mg/ml ZnO nanoparticle solution in ethanol onto the QD layers at 2000 rpm and annealing at 100 °C for 30 min in the same glove box to remove the residual solvent. Finally, these substrates were quickly loaded into a vacuum chamber for Al cathode fabrication at a pressure below 4×10^{-6} Torr. Al cathode lines (2.5 mm wide) were deposited orthogonally to the 2 mm ITO anode lines to form a 5 mm^2 active area.

4.2 Photoelectrical properties of the QLEDs. Current–voltage and luminance characteristics were measured by a programmable Keithley model 2400 power supply and a Minolta Luminance Meter LS-110, respectively. The spectra of the devices were recorded with an Ocean Optics Maya 2000-Pro spectrometer. All the measurements were taken in air at room temperature

4.3 Structural and optical characterization of nanoparticles and films. Room-temperature PL spectra of the QDs in toluene were also collected using an Ocean Optics Maya 2000-Pro spectrometer under an excitation wavelength of 405 nm. TRPL measurements were performed with an Edinburgh Instruments FL920 spectrometer

using a 400 nm excitation light source. XPS spectra were measured by a Kratos Axis-Ultra spectrometer (a monochromatic Al Kα source and 15 kV/8 mA). The morphology of the QD layers on s-NiO and s-NiO/Al_2O_3 films was characterized by SEM (Hitachi S4800). AFM images were recorded in tapping mode on a Bruker Multimode-8 microscope. The Kelvin probe measurements were performed using a SKP5050 (KP Technology Ltd).

Acknowledgements

This work was supported by the program of the National Natural Science Foundation of China (Nos. 11674315 and 11704150).

Author contributions

W.J. and H.S. conceived the device design. W.J. and J.F. analyzed the data under the supervision of H.S. W.J. wrote the manuscript. H.S. synthesized the QDs. Q.Y., H.Z., and Z.K. carried out the steady-state and time-resolved experiments. J.F., H.S. and H.Z.Z. commented significantly on the experiments and data analysis. All authors reviewed the manuscript and discussed the results.

References

[1] L. E. Brus, Electron-electron and electron-hole interactions in small semiconductor crystallites-the size dependence of the lowest excited electronic state. *J. Chem. Phys.* **1984**, *80*, 4403-4409.

[2] Y. Masumoto, K. Sonobe, Size-dependent energy levels of CdTe quantum dots. *Phys. Rev. B* **1997**, *56*, 9734-9737.

[3] G. D. Scholes, G. Rumbles, Excitons in nanoscale systems. *Nat. Mater.* **2006**, *5*, 683-696.

[4] X. Y.Liang, S. Bai, X. Wang, X. L. Dai, F. Gao, B. Q. Sun, Z. J. Ning, Z. Z. Y. Z. Jin, Colloidal metal oxide nanocrystals as charge transporting layers for solution-processed light-emitting diodes and solar cells. *Chem, Soc. Rev.* **2017**, *46*, 1730-1759.

[5] X. L. Dai, Z. X. Zhang, Y. Z. Jin, Y. Niu, H. J. Cao, X. Y. Liang, L. W. Chen, J. P. Wang, X. G. Peng, Solution-processed, high-performance light-emitting diodes based on quantum dots. *Nature* **2014**, *515*, 96–100.

[6] M. V. Kovalenko, L. Manna, A. Cabot, Z. Hens, D. V. Talapin, C. R. Kagan, V. I. Klimov, A. L. Rogach, P. Reiss, D. J. Milliron, P. Guyot-Sionnnest, G. Konstantatos, W. J. Parak, T. Hyeon, B. A. Korgel, C. B. Murray, W. Heiss. Prospects of nanoscience with nanocrystals. *ACS Nano,* **2015**, *9*, 1012-1057.

[7] C. R. Kagan, E. Lifshitz, E. H. Sargent, D. V. Talapin, Building devices from colloidal quantum dots. *Science* **2016**, *353*, 885-.

[8] W. Y. Ji, T. Wang, B. Y. Zhu, H. Zhang, R. Wang, D. D. Zhang, L. Z. Chen,

Q. Yang, and H. Z. Zhang, Highly efficient flexible quantum-dot light emitting diodes with an ITO/Ag/ITO cathode, *J. Mater. Chem. C* **2017**, *5*, 4543–4548.

[9] T. Erdem, H. V. Demir, Colloidal nanocrystals for quality lighting and displays: milestones and recent developments. in *Nanophotonics* **2016**, *5*, 74-95.

[10] R. M. Yu, F. R. Yin, X. Y.Huang and W. Y. Ji, Molding hemispherical microlens arrays on flexible substrates for highly efficient inverted quantum dot light emitting diodes, *J. Mater. Chem. C* **2017**, *5*, 6682–6687.

[11] H. Z. Zhong, Z. L. Bai, B. S. Zou, Tuning the luminescence properties of colloidal I-III-VI semiconductor nanocrystals for optoelectronics and biotechnology applications. *J. Phys. Chem. Lett.* **2012**, *3*, 3167-3175.

[12] F. Zhang, H. Z. Zhong, C. Chen, X. G. Wu, X. M. Hu, H. L. Huang, J. B. Han, B. S. Zou, Y. P. Dong, Brightly luminescent and color-tunable colloidal $CH_3NH_3PbX_3$ (X = Br, I, Cl) quantum dots: potential alternatives for display technology. *ACS Nano* **2015**, *9*, 4533-4542.

[13] H. L. Huang, F. C. Zhao, L. G. Liu, F. Zhang, X. G. Wu, L. J. Shi, B. S. Zou, Q. B. Pei, H. Z. Zhong, Emulsion synthesis of size-tunable $CH_3NH_3PbBr_3$ quantum dots: an alternative route toward efficient light-emitting diodes. *ACS Appl. Mater. Interfaces* **2015**, *7*, 28128-28133.

[14] Y. Shang, Z. Ning, Colloidal quantum dots surface and device structure engineering for high performance light emitting diodes. *Natl. Sci. Rev.* Jan. **2017**.

[15] Z. L. Bai, H. Z. Zhong, Halide perovskite cuantum dots: potential candidates

for display technology. *Science Bulletin* **2015**, *60*, 1622-1624.

[16] S. Reineke, Complementary LED technologies. *Nat. Mater.* **2015**, *14*, 459-462.

[17] H. B. Shen, W. R. Cao, N. T. Shewmon, C. C. Yang, L. S. Li, J. G. Xue, High-efficiency, low turn-on voltage blue-violet quantum-dot-based light-emitting diodes. *Nano Lett.* **2015**, *15*, 1211-1216.

[18] Y. X. Yang, Y. Zheng, W. R. Cao, A. Titov, J. Hyvonen, J. R. Manders, J. G. Xue, P. H. Holloway, L. Qian, High-efficiency light-emitting devices based on quantum dots with tailored nanostructures. *Nat. Photonics* **2015**, *9*, 259-266.

[19] E. Matioli, S. Brinkley, K. Kelchner, Y. Hu, S. Nakamura, S. DenBaars, J. Speck, C. Weisbuch, High-brightness polarized light-emitting diodes. *Light Sci. Appl.* **2012**, 1, e22.

[20] C. Xiang, W. Koo, F. So, H. Sasabe, J. Kido, A systematic study on efficiency enhancements in phosphorescent green, red and blue microcavity organic light emitting devices. *Light Sci. Appl.* **2013**, 2, e74.

[21] D. Bozyigit, V. Wood, Challenges and solutions for high-efficiency quantum dot-based LEDs. *MRS Bull.* **2013**, *38*, 731-736.

[22] L. Qian, Y. Zheng, J. Xue, P. H. Holloway, Stable and efficient quantum-dot light-emitting diodes based on solution-processed multilayer structures. *Nat. Photonics* **2011**, *5*, 543−548.

[23] J. H. Kwak, W. K. Bae, D. G. Lee, I. Park, J. H. Lim, M. J. Park, H. D. Cho, H. J. Woo, D. Y. Yoon, K. H. Char, S. H. Lee, C. H. Lee, Bright and efficient

full-color colloidal quantum dot light-emitting diodes using an inverted device structure. *Nano Lett.* **2012**, *12*, 2362–2366.

[24] B. S. Mashford, M. Stevenson, Z. Popovic, C. Hamilton, Z. Zhou, C. Breen, J. Steckel, V. Bulović, M. G. Bawendi, S. Coe-Sullivan, P. T. Kazlas, High-efficiency quantum-dot light-emitting devices with enhanced charge injection. *Nat. Photonocs* **2013**, *7*, 407-412.

[25] T. H. Kim, K. S. Cho, E. K. Lee, S. J. Lee, J. Chae, J. W. Kim, D. H. Kim, J. Y. Kwon, G. Amaratunga, S. Y. Lee, B. L. Choi, Y. Kuk, J. M. Kim, K. Kim, Full-color quantum dot displays fabricated by transfer printing. *Nat. Photonics* **2011**, *5*, 176-182.

[26] K. S. Cho, E. K. Lee, W. J. Joo, E. Jang, T. H. Kim, S. J. Lee, S. J. Kwon, J. Y. Han, B. K. Kim, B. L. Choi, J. M. Kim, High-performance crosslinked colloidal quantum-dot light-emitting diodes. *Nat. Photonics* **2009,** *3*, 341-345.

[27] W. Y. Ji, P. T. Jing, J. L. Zhao, X. Liu, A. Wang, H. Li, Inverted CdSe/CdS/ZnS quantum dot light emitting devices with titanium dioxide as an electron-injection contact. *Nanoscale* **2013**, *5*, 3474−3480.

[28] J. M. Caruge, J. E. Halpert, V. Wood, V. Bulovic, M. G. Bawendi, Colloidal quantum-dot light-emitting diodes with metal-oxide charge transport layers. *Nat. Photonics* **2008,** *2*, 247-250.

[29] J. M. Caruge, J. E. Halpert, V. Bulovic, M. G. Bawendi, NiO as an inorganic hole-transporting layer in quantum-dot light-emitting devices. *Nano Lett.* **2006,** *6*, 2991-2994.

[30] W. Y. Ji, S. H. Liu, H. Zhang, R. Wang, W. F. Xie, H. Z. Zhang, Ultrasonic spray processed, highly efficient all-inorganic quantum dot light emitting diodes. *ACS Photonics* **2017**, *4*, 1271–1278.

[31] B. S. Mashford, T. L. Nguyen, G. J. Wilson, P. Mulvaney, All-inorganic quantum-dot light-emitting devices formed via low-cost, wet-chemical processing. *J. Mater. Chem.* **2010**, *20*, 167-172.

[32] W. J. Ji, Y. Tian, Q. H. Zeng, S. N. Qu, L. G. Zhang, P. T. Jing, J. Wang, J. L. Zhao, Efficient quantum dot light emitting diodes by controlling the carrier accumulation and exciton formation. *ACS Appl. Mater. Interfaces* **2014**, *6*, 14001-14007.

[33] J. Lim, B. G. Jeong, M. Park, J. K. Kim, J. M. Pietryga, Y.-S. Park, V. I. Klimov, C. Lee, D. C. Lee, W. K. Bae, Influence of shell thickness on the performance of light-emitting devices based on CdSe/$Zn_{1-X}Cd_XS$ core/shell heterostructured quantum dots. *Adv. Mater.* **2014**, *26*, 8034–8040.

[34] K. T. Shimizu, W. K. Woo, B. R. Fisher, H. J. Eisler, M. G. Bawendi, Surface-enhanced emission from single semiconductor nanocrystals. *Phys. Rev. Lett.* **2002**, *89*, 117401.

[35] E. L. Ratcliff, J. Meyer, K. X. Steirer, A. Garcia, J. J. Berry, D. S. Ginley, D. C. Olson, A. Kahn, N. R. Armstrong, Evidence for near-surface NiOOH species in solution-processed NiO*x* selective interlayer materials: impact on energetics and the performance of polymer bulk heterojunction photovoltaics. *Chem. Mater.* **2011**, *23*, 4988−5000.

[36] C.-L. Chiang, S.-M. Tseng, C.-T. Chen, C.-P. Hsu, C.-F. Shu, Influence of molecular dipoles on the photoluminescence and electroluminescence of dipolar spirobifluorenes. *Adv. Funct. Mater.* **2008**, *18*, 248–257.

[37] R. L. Puurunen, Surface chemistry of atomic layer deposition: a case study for the trimethylaluminum/water process, *J. Appl. Phys.* **2005**, *97*, 121301.

[38] B. Hoex, J. Schmidt, P. Pohl, M. C. M. van de Sanden, W. M. M. Kessels, Silicon surface passivation by atomic layer deposited Al_2O_3. *J. Appl. Phys.* **2008**, *104*, 044903.

[39] V. Wood, M. J. Panzer, J. M. Caruge, J. E. Halpert, M. G. Bawendi, V. Bulovic, Air-stable operation of transparent, colloidal quantum dot based LEDs with a unipolar device architecture. *Nano Lett.* **2010**, *10*, 24–29.

[40] Y. Shirasaki, G. J. Supran, W. A. Tisdale, V. Bulovic, Origin of efficiency roll-off in colloidal quantum-dot light-emitting diodes. *Phys. Rev. Lett.* **2013**, *110*, 217403.

[41] S. A. Empedocles, M. G. Bawendi, Quantum-confined stark effect in single CdSe nanocrystallite quantum dots. *Science* **1997**, *278*, 2114.

[42] J. Seufert, M. Obert, M. Scheibner, N. A. Gippius, G. Bacher, A. Forchel, Stark effect and polarizability in a single CdSe/ZnSe quantum dot. *Appl. Phys. Lett.* **2001**, *79*, 1033-1035.

[43] S. Liu, R. Liu, Y. Chen, S. Ho, J. H. Kim, F. So, Nickel oxide hole injection/transport layers for efficient solution-processed organic light-emitting diodes, *Chem. Mater.* **2014**, *26*, 4528−4534.

[44] Y. Louyer, L. Biadala, P. Tamarat, B. Lounis, Spectroscopy of neutral and charged exciton states in single CdSe/ZnS nanocrystals, *Appl. Phys. Lett.* **2010**, *96*, 203111.

[45] H. Ibuki, T. Ihara, Y. Kanemitsu, Spectral diffusion of emissions of excitons and trions in single CdSe/ZnS nanocrystals: charge fluctuations in and around nanocrystals. *J. Phys. Chem. C* **2016**, *120*, 23772−23779.

[46] W. Y. Ji, P. T. Jing, L. G. Zhang, D. Li, Q. H. Zeng, S. N. Qu, J. L. Zhao, The work mechanism and sub-bandgap-voltage electroluminescence in inverted quantum dot light-emitting diodes, *Sci. Rep.* **2014**, *4*, 6974.

[47] C. R. Kagan, C. B. Murray, M. G. Bawendi, Long-range resonance transfer of electronic excitations in close-packed CdSe quantum-dot solids. *Phys. Rev. B* 54, 8633–8643 (1996).

[48] H. B. Shen, S. Wang, H. Z. Wang, J. Z. Niu, L. Qian, Y. X. Yang, A. Titov, J. Hyvonen, Y. Zheng, L. S. Li, Highly efficient blue−green quantum dot light-emitting diodes using stable low-cadmium quaternary-alloy ZnCdSSe/ZnS core/shell nanocrystals. *ACS Appl. Mater. Interfaces* **2013**, *5*, 4260−4265.

[49] J. R. Manders, S.-W. Tsang, M. J. Hartel, T.-H. Lai, S. Chen, C. M. Amb, J. R. Reynolds, F. So Solution-processed nickel oxide hole transport layers in high efficiency polymer photovoltaic cells. *Adv. Funct. Mater.* **2013**, *23*, 2993-3001.

Figure captions

Figure 1. Schematic diagram of (a) the device structure and (b) the passivating mechanism.

Figure 2. XPS spectra of (a) s-NiO and (b) s-NiO/Al_2O_3 thin films.

Figure 3. AFM images of (a) pure s-NiO, and s-NiO with various cycles of Al_2O_3 deposition: (b) 0.45 nm, (c) 0.9 nm, and (d) 1.35 nm. The corresponding RMS values of the samples are 1.62, 1.58, 1.43, and 1.43 nm, respectively.

Figure 4. Photoelectric properties of QLEDs. (a) Voltage versus current density (*V*–*J*), (b) voltage versus luminance (*V*–*L*), (c) current density–luminous efficiency, and (d) current density–external quantum efficiency.

Figure 5. Spectroscopic characterization of devices and QDs in films. (a) EL spectra of different devices at 4.5 V, as well as the PL spectra of QD film on glass and QDs in toluene. (b) EL spectra of device C driven under different voltages. The inset shows a photograph of the device at an operating voltage of 4.5 V. (c) Time-resolved and (d) steady-state PL spectra of QD layers on s-NiO substrates with Al_2O_3 layers of 0, 0.45, 0.9, and 1.35 nm in thickness. TRPL spectra of QDs in toluene and on a glass substrate are also shown for reference. The inset shows UV-illuminated photographs of QD films on s-NiO with Al_2O_3 thicknesses of 0–1.8 nm, which exhibit an identical trend to the PL intensities in Figure 5c.

Table caption

Table 1 Optical properties of QDs in different environments.

Figure 1

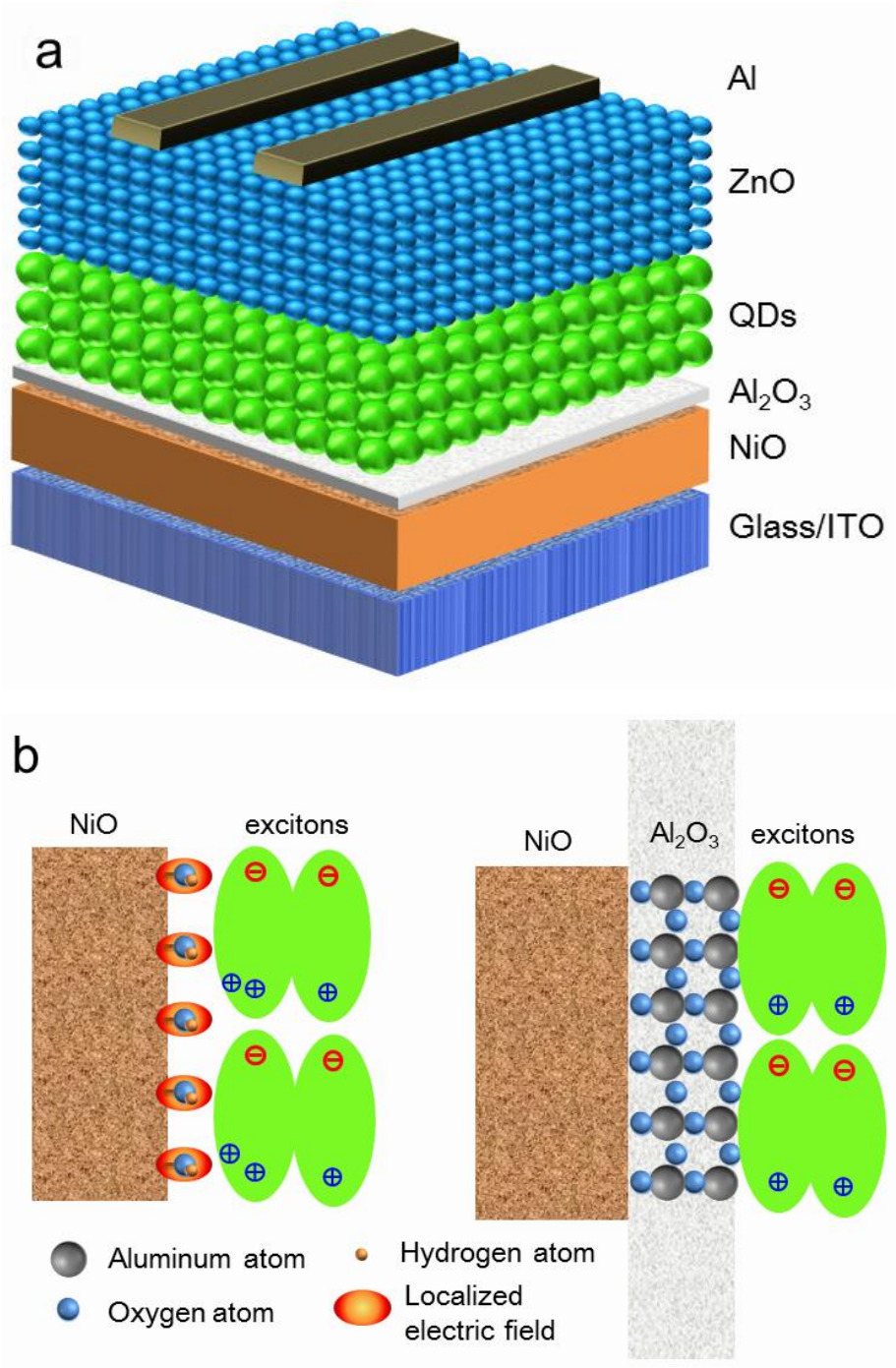

Figure 1. Schematic diagram of (a) the device structure and (b) the passivating mechanism.

Figure 2

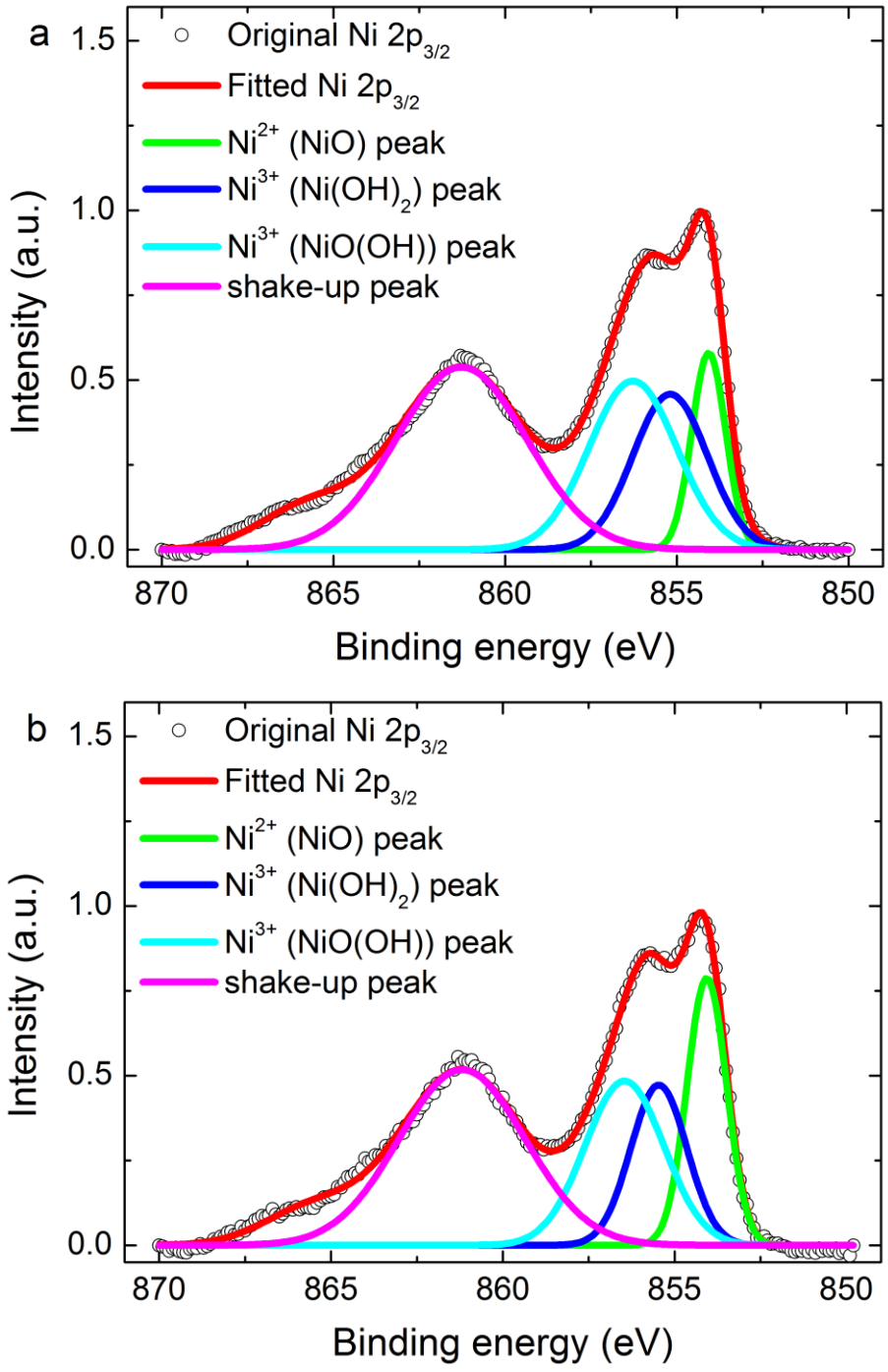

Figure 2. XPS spectra of (a) s-NiO and (b) s-NiO/Al_2O_3 thin films.

Figure 3

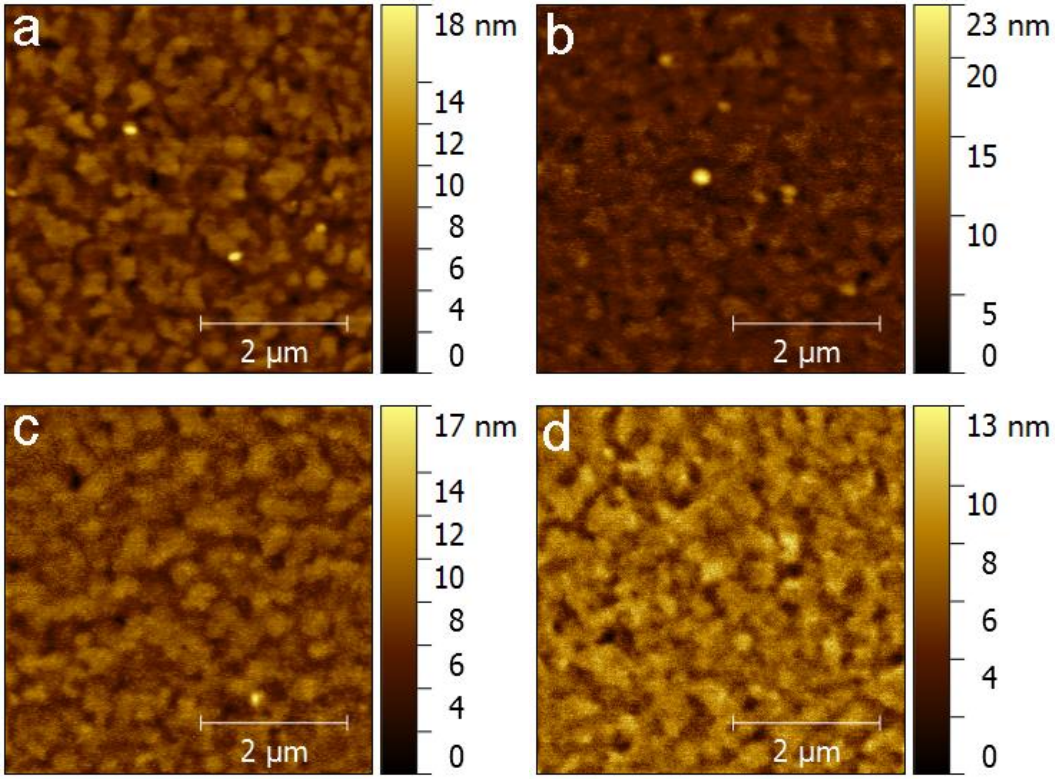

Figure 3. AFM images of (a) pure s-NiO, and s-NiO with various cycles of Al_2O_3 deposition: (b) 0.45 nm, (c) 0.9 nm, and (d) 1.35 nm. The corresponding RMS values of the samples are 1.62, 1.58, 1.43, and 1.43 nm, respectively.

Figure 4

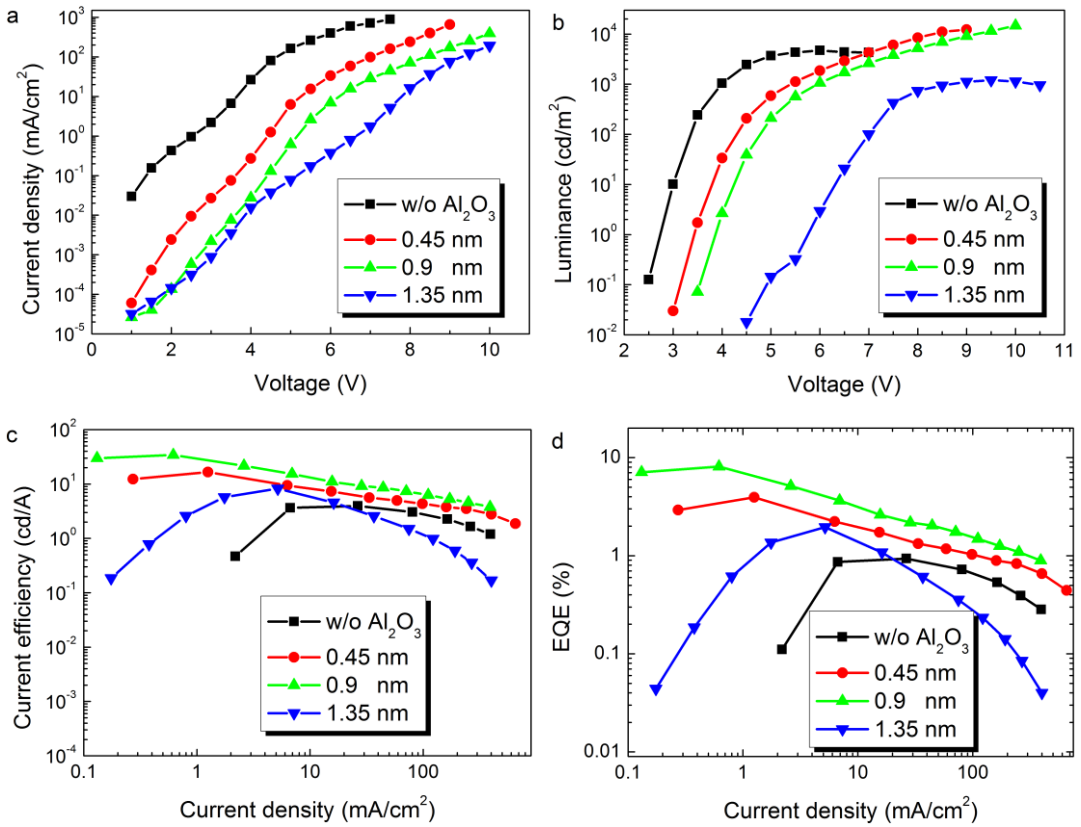

Figure 4. Photoelectric properties of QLEDs. (a) Voltage versus current density (*V*-*J*), (b) voltage versus luminance (*V*-*L*), (c) current density-luminous efficiency, and (d) current density-external quantum efficiency.

Figure 5

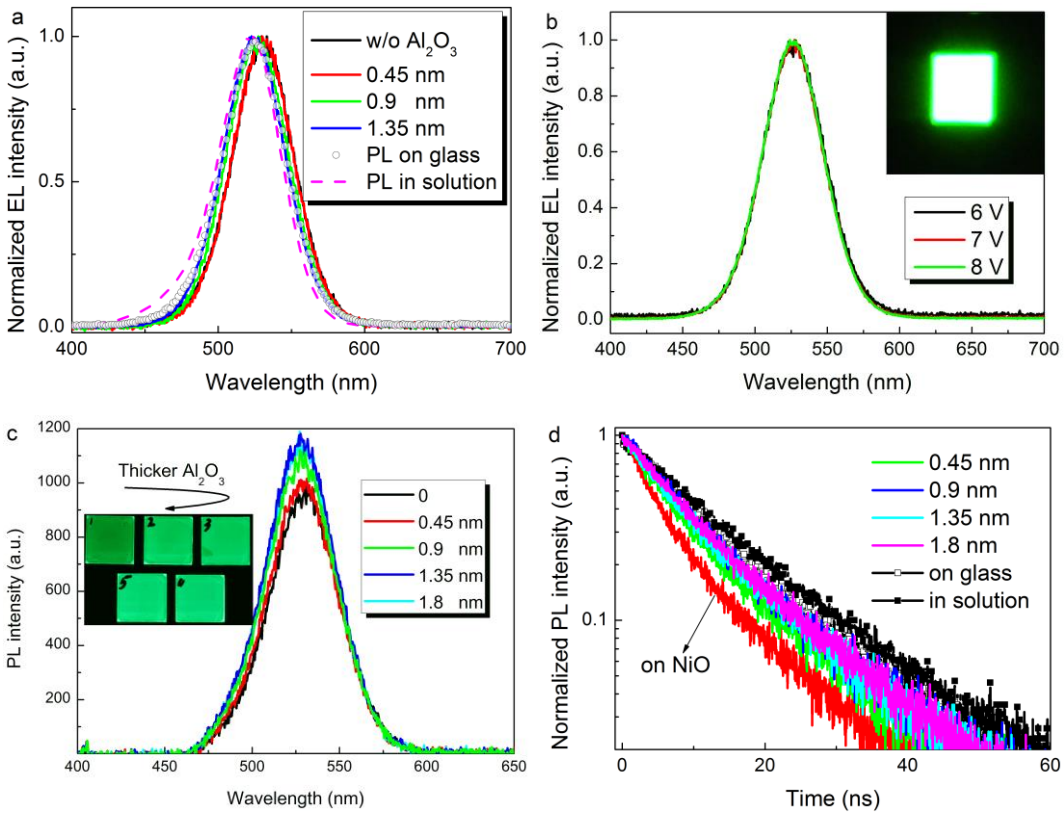

Figure 5. Spectroscopic characterization of devices and QDs in films. (a) EL spectra of different devices at 4.5 V, as well as the PL spectra of QD film on glass and QDs in toluene. (b) EL spectra of device C driven under different voltages. The inset shows a photograph of the device at an operating voltage of 4.5 V. (c) Time-resolved and (d) steady-state PL spectra of QD layers on s-NiO substrates with Al_2O_3 layers of 0, 0.45, 0.9, and 1.35 nm in thickness. TRPL spectra of QDs in toluene and on a glass substrate are also shown for reference. The inset shows UV-illuminated photographs of QD films on s-NiO with Al_2O_3 thicknesses of 0–1.8 nm, which exhibit an identical trend to the PL intensities in Figure 5c.

Table 1 Optical properties of QDs in different environments.

Samples	Average lifetime (ns)	PL peak (nm)	EL peak (nm)
NiO/QDs	9.85	530.7	530.0
NiO/Al_2O_3/(0.45 nm)/QDs	11.43	529.2	529.6
NiO/Al_2O_3/(0.9 nm)/QDs	12.01	527.8	527.3
NiO/Al_2O_3/(1.35 nm)/QDs	12.38	527.3	526.1
NiO/Al_2O_3/(1.8 nm)/QDs	12.55	527.3	-
Glass/QDs	13.42	526.2	-
QDs in toluene	15.01	522.4	-